Eur. Phys. J. B **52**, 163–170 (2006)
DOI: 10.1140/epjb/e2006-00289-3

THE EUROPEAN PHYSICAL JOURNAL B

Molecular Dynamics as a tool to interpret macroscopic amorphization-induced swelling in silicon carbide

F. Ribeiro[1], E. Castelier[1], M. Bertolus[1,a], and M. Defranceschi[2]

[1] Commissariat à l'Énergie Atomique, Direction de l'énergie nucléaire; DEC/SESC/LLCC, Bâtiment 151, CE Cadarache, 13108 Saint-Paul-lez-Durance, France
[2] Commissariat à l'Énergie Atomique, Direction de l'énergie nucléaire; DSOE/RB, Bâtiment 121, CE Saclay, 91191 Gif-sur-Yvette Cedex, France

Received 22 February 2006
Published online 31 July 2006 –

Abstract. We present here an investigation of the irradiation-induced swelling of SiC using Classical Molecular Dynamics simulations. Heavy ion irradiation has been assumed to affect the material in two steps: (a) creation of local atomic disorder, modeled by the introduction of extended amorphous areas with various sizes and shapes in a crystalline SiC sample at constant volume (b) induced swelling, determined through relaxation using Molecular Dynamics at constant pressure. This swelling has been computed as a function of the amorphous fraction introduced. Two different definitions of the amorphous fraction were introduced to enable meaningful comparisons of our calculations with experiments and elastic modeling. One definition based on the displacements relative to the ideal lattice positions was used to compare the Molecular Dynamics results with data from experiments combining ion implantations and channeled Rutherford Backscattering analyses. A second definition based on atomic coordination was used to compare the Molecular Dynamics results to those yielded by a simplified elastic model. The simulation results using the lattice-based definition of the amorphous fraction compare very well with the experimental results. This proves that the modeling in two steps chosen for the creation of the amorphous regions is reasonable. Moreover, the results show very clearly that SiC swelling does not scale linearly with the amorphous fraction introduced. Two swelling regimes are observed relatively to the size of the amorphous area. Comparison of the elastic model with the Molecular Dynamics results using the coordination-based definition of the amorphous fraction has also enabled us to shed light on the swelling mechanisms and has shown that amorphization-induced swelling exhibits an elastic behavior. Furthermore, scalings for the swelling as a function of the two amorphous fractions considered, which can be used by larger scale models, have been determined. Finally, our study shows that classical Molecular Dynamics calculations enable one to connect the results of the available experiments with the elastic calculations and to get further insight into the swelling mechanisms.

PACS. 31.15.Qg Molecular dynamics and other numerical methods – 61.80.Jh Ion radiation effects – 62.20.Dc Elasticity, elastic constants

1 Introduction

The evolution of structural and mechanical properties of materials in high-radiation environment is a significant issue in nuclear applications. In particular, irradiation-induced swelling has important consequences which can affect considerably the material performance. Numerous experimental studies of volume changes in ceramics under irradiation have been published over the years [1]. For example, ion implantation experiments combined with Rutherford Backscattering analysis [2,3] have been performed on silicon carbide. These studies tend to show that material swelling under irradiation is a complex phenomenon. In particular, SiC swelling does not depend linearly on the disorder created in the material, but exhibits two different scalings as a function of this disorder. The atomic-scale mechanisms behind this scaling change are not well understood.

Several processes at various scales take part to this swelling: creation of point defects, local amorphization, intra or intergranular void creation, gas formation... The creation and migration of point defects in semiconductors and particularly SiC have been studied extensively using empirical [4–7] or *ab initio* methods [8–12]. On the

[a] e-mail: marjorie.bertolus@cea.fr

contrary, there are very few studies on the influence of the creation of extended disordered or amorphous zones on the material swelling [13,14] and it is currently the least well known atomic-scale component of the irradiation-induced swelling. Atomistic modeling enables us to separate the various phenomena and can therefore be a powerful tool to shed light on their respective influences. The present study focuses on amorphization-induced swelling. We are particularly interested in getting further insight into atomic-scale mechanisms, as well as in determining a scaling law of this swelling as a function of the fraction of amorphous material created. Such a law could be used in multiscale models of materials behavior under irradiation.

In this study heavy ion irradiation is assumed to induce only local amorphization, and to affect the material in two successive steps: (1) creation of local amorphous disorder at constant volume, (2) volume relaxation and induced swelling. A preliminary study of amorphization-induced swelling using this methodology has been published previously [15]. The results of this study have shown that the modeling chosen is able to reproduce the available experimental results, in particular the two regimes observed in the evolution of the volume change as a function of the amorphous fraction introduced. The precise swelling mechanisms, as well as the influence of the structure of the interface and of the amorphous area, however, were not completely elucidated. The aim of the present paper is to answer the open questions left by this preliminary study, and in particular determine the swelling mechanisms. To this aim we have considered a more physical amorphization method as in the previous study, and have determined the swelling obtained as a function of the disorder introduced. We have also performed continuum calculations using an elastic model. We have finally compared the results yielded by the Classical Molecular Dynamics and the elastic calculations to the experimental results.

The outline of the paper is as follows. We expose first the computational details: choice of atomistic modeling, amorphization method, possible definitions for the amorphous fraction introduced, as well as description of the elastic calculations. Then we present the results obtained on the swelling as a function of the amorphous fraction introduced, and finally the conclusions of the comparison with the experimental and elastic results.

2 Computational details

2.1 Atomistic modeling chosen

We must first choose a methodology for the investigation. We want to study the swelling induced by the introduction of various fractions of amorphous material ranging from a few percent to over half of amorphous material. The system considered must therefore be large enough to enable the introduction, on the one hand of very small fractions of disordered material but containing enough atoms to be amorphous, and on the other hand large amorphous fractions while avoiding spurious interactions between images in the periodic representation. A simulation box containing several thousands of atoms is therefore necessary. Second, given the various amorphous fractions to consider, our study implies a rather large number of simulations. Third, to investigate the swelling mechanisms, we need a dynamical method to follow the system evolution in time over a few picoseconds. The combination of number of calculations, size of simulation box, and simulation times excludes at the moment an *ab initio* treatment. Furthermore, successful empirical potentials have been developed for SiC, in particular Tersoff potentials [16], which enable the accurate study of defects in SiC using Classical Molecular Dynamics simulations [17–19]. We have therefore chosen to use a Classical Molecular Dynamics approach.

2.2 Molecular Dynamics code and empirical potential

All simulations reported herein were carried out using the Molecular Dynamics simulation code XMD. This code has been developed by Rifkin and is freely available on the web [20]. This code enables both constant volume and constant pressure isothermal simulations (in NVT and NPT ensembles) under periodic boundary conditions. The timestep chosen is 0.1 fs at 5500 K and 0.25 fs at 300 K. The temperature control is achieved by a clamp algorithm involving a rescaling of the velocities. Similarly, the pressure control is achieved by a pressure clamp algorithm, i.e. internal stress calculations and rescaling of the lattice parameters. Furthermore, it is possible to apply different temperature and pressure conditions in different parts of the system.

Besides, the XMD code allows the use of different interatomic potentials. We have decided to use Tersoff potentials, which enable a good description of crystalline [16] and amorphous [21] SiC. The 89' version of the Tersoff potential [16] is implemented in the program, and we have added the 94' version [21] to test the influence of the potential parametrization on our results. No qualitative difference is observed between the two series of simulations. Therefore only the results obtained with the 89' parametrization are presented here.

2.3 Local amorphization and relaxation

The introduction of the amorphous area was performed by amorphizing the central area of the supercell in situ at constant volume. To do this we have separated the system in two sub-systems. To free ourselves from border and corner effects in the interface between the crystalline and amorphous areas, central areas with spherical and cubic shape have been considered. The central area is melted at 5500 K during 60 ps and is then cooled down to 300 K using a velocity rescaling over 33 timesteps. It becomes amorphous. We have checked that the amorphous structure obtained is independent from the scheme used to lower the temperature. The same properties were obtained using a formal quenching scheme (velocity of atoms put to zero as soon as their energy increases) or by a clamp over

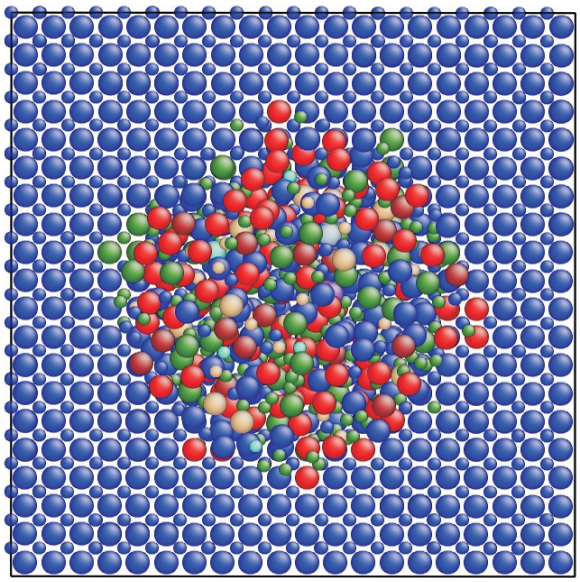

Fig. 1. Composite sample obtained in the case of a spherical in situ melted quenched zone. Large and small spheres represent Si and C atoms, respectively. Color coding is done according to coordination number: blue, red, and green correspond to coordination numbers four, five, and three, respectively.

333 timesteps. The parameters chosen allow for the shortest relaxation time, the equilibrium at 300 K is reached in approximately 5 ps. The outside area is first fixed at 0 K during the first 60 ps, then relaxed to 300 K using the same clamp scheme as the amorphous zone, and remains crystalline. In this manner the crystalline part of the material is taken into account during the amorphization of the central region. The interface produced is therefore different from the interface yielded by the "cut-paste" method used in the preliminary study [15], and should give a better representation of the system physics. The composite sample obtained in the case of a spherical *in situ* melted quenched zone has been represented in Figure 1 using the AtomEye software [22]. On this figure large and small spheres represent Si and C atoms, respectively. Color coding is done according to coordination number: blue, red, and green correspond to coordination numbers four, five, and three, respectively.

The composite samples obtained are finally allowed to relax in NPT ensemble at 300 K for 400 ps.

2.4 Simulation box and amorphous fractions considered

We have chosen a simulation box with initial dimension $V^0 = 10\,a \times 10\,a \times 10\,a$, where a is the β-SiC lattice parameter at 0 K and equal to 4.32 Å in the potential used. The simulation box contains a constant number of atoms: 8000. Thanks to the periodic boundary conditions used in the program this enables us to model a perfect and infinite SiC monocrystal. The amorphous fractions considered vary from a few percents to about 60%. These fractions are the highest amorphous fractions that can be introduced in the supercell if we want to avoid spurious interactions between images in the Periodic Boundary Conditions.

2.5 Elastic model

In order to elucidate the swelling mechanisms we have compared the Molecular Dynamics results with the elastic theory. To this aim we have studied using elastic theory the simplified case of a sphere of amorphous material included in a hollow sphere of crystalline material with no surface tension at the interface. Both materials are supposed to be homogeneous and isotropic. The system considered is represented in Figure 2. The volumes of amorphous and crystalline materials are respectively V_a and V_c, and the total volume is:

$$V = V_a + V_c, \tag{1}$$

which is V^0 initially. An external pressure p_c equal to zero is applied to the system.

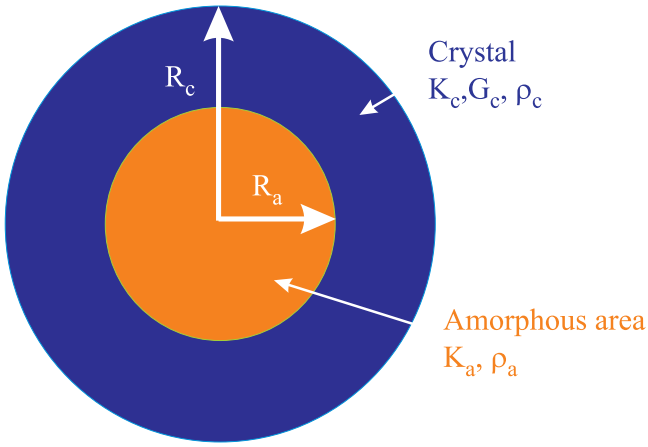

Fig. 2. Amorphous sphere of radius R_a included in a crystalline sphere of radius R_c.

Before volume relaxation the density in the two parts of the system is the same and equal to the crystalline density at rest ρ_c^r. After relaxation, the density of the amorphous phase becomes ρ_a^f inducing a pressure p^a within this sphere, and a swelling of the total system. This swelling is characterized by the relative volume change:

$$\frac{\Delta V}{V^0} = \frac{V^f - V^0}{V^0} \tag{2}$$

where superscripts 0 and f denote the initial and final states of the system.

The volume change can be obtained by solving the equilibrium equation of the system. The swelling can then be expressed as a function of the volumic amorphous fraction in the initial state ϕ^0 defined as:

$$\phi^0 = \frac{V_a^0}{V^0}, \tag{3}$$

of the densities ρ_a^r and ρ_c^r of the amorphous and crystalline materials at rest, respectively, as well as of the bulk and shear moduli, K_a, K_c and G_c. The details of the model developed for this study and of the calculations are reported in the appendix. The final expression obtained for the swelling of the system is:

$$\frac{\Delta V}{V^0} = \frac{(\rho_c^r - \rho_a^r)\, K_a\, (3\, K_c + 4\, G_c)\, \phi^0}{K_c\, (4\, \rho_c^r\, G_c + 3\, \rho_a^r\, K_a) + 4\, G_c\, (\rho_a^r\, K_a - \rho_c^r\, K_c)\, \phi^0}. \tag{4}$$

The elastic moduli K_c, G_c, K_a, the densities ρ_c^r, ρ_a^r were calculated at 300 K using the implementation of classical Molecular Dynamics and the parameters described in section 2.2. A totally amorphous sample with size $V^0 = 10\,a \times 10\,a \times 10\,a$, was prepared in melting and quenching, then allowed to relax at constant pressure over 400 ps. The cell parameter was averaged on the 5000 final timesteps to allow for volume relaxation. The density ρ_a^r is then calculated using the cell parameter obtained. The elastic moduli have been determined numerically. The cell volumes for the crystal and for an amorphous sample prepared as described above have been determined for various pressures. The bulk moduli were then calculated according to the definition:

$$\frac{1}{K} = -\frac{1}{V}\frac{dV}{dP}. \tag{5}$$

The values obtained can be found in Table 1.

Table 1. Values of the parameters of the elastic calculations K_c, K_a, G_c, ρ_c^r and ρ_a^r yielded by the Molecular Dynamics simulations.

K_c (GPa)	K_a (GPa)	G_c (GPa)	ρ_c^r (kg m^{-3})	ρ_c^r (kg m^{-3})
300	180	195	3.26	2.95

2.6 Definition of the amorphous fraction introduced

The objective of our investigation is to determine the relative volume change $\Delta V/V^0$, or swelling, induced by the introduction of amorphous areas with various sizes in the material. The swelling expression is given by equation (2). The crucial point is then to determine the proportion of amorphous material. It is not straightforward, however, since there is no unequivocal definition of an amorphous atom, the amorphous state being essentially a collective property. To determine the amorphous fraction as precisely as possible we have therefore chosen to use two different definitions of an amorphous atom. The first definition of the amorphous fraction, referred to as the lattice amorphous fraction $f_{a\,\mathrm{lattice}}$, is based on the analysis of the positions of the atoms in the configuration after relaxation compared to their ideal positions in the perfect crystal lattice. We consider as amorphous each atom i for which the atomic displacement relative to the lattice site is greater than a threshold distance α. This displacement is calculated as $dr = |r_i - r_i^0|$, where r_i is the position in the sample after relaxation and r_i^0 the ideal lattice position in a crystal with the same lattice parameter as the relaxed cell. Based on the $|r_i - r_i^0|$ distribution of atomic positions in $\beta-$SiC at 300 K represented in Figure 3, we have chosen $\alpha = 0.16$ Å. This definition may theoretically underestimate the amorphous fraction since an amorphous atom can by chance sit on a lattice site. But this is very rare in practice, and $f_{a\,\mathrm{lattice}} = 99.9\% \approx 100\%$ for a fully amorphous cell obtained by a melting-quench process. The main objective of this amorphous fraction definition is to enable a direct comparison with the results from Rutherford Back Scattering (RBS) experiments on irradiated SiC-samples. In RBS combined with channeling techniques the monocrystalline substrate is aligned with the incident ion beam. The backscattering yield then depends on the fraction of atoms which are not in lattice sites, and the disordered fraction determined in these experiments is then based on a position criterion. The lattice amorphous fraction is computed after volume relaxation to be consistent with the experiments, which can only access the final state.

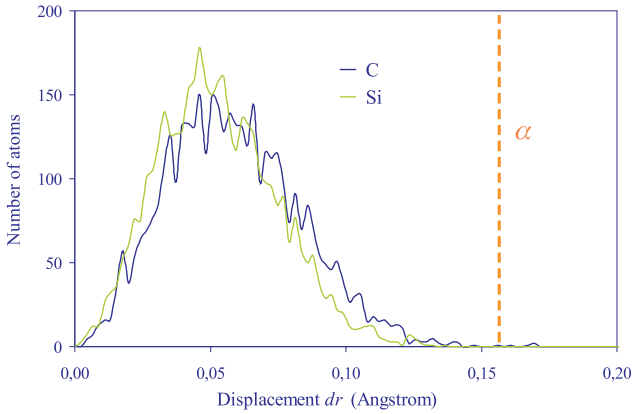

Fig. 3. $dr = |r_i - r_i^0|$ distribution of atomic positions in $\beta-$SiC at 300 K.

The second definition, referred to as the coordination amorphous fraction $f_{a\,\mathrm{coord}}$, is based on the analysis of the atomic coordination numbers. The coordination numbers are calculated using a distance criterion: C–C, C–Si and Si–Si bonds are considered to be formed if the two atoms involved are closer than 1.70, 2.10, and 2.80 Å, respectively. These thresholds were determined through the analysis of the distance distributions in various Si–C systems. Then only atoms exhibiting exactly four heteronuclear bonds and no homonuclear bond are considered crystalline, all the others being amorphous. We have checked that taking into account bond angles does not modify the value of $f_{a\,\mathrm{coord}}$. This definition seems the most physical since it is based on interatomic interactions and bonding, which is at the origin of the materials properties. It is not perfect, however, since an atom can exhibit an ideal first coordination sphere, but no order in its second coordination sphere. Such an atom will be wrongly considered as crystalline using this second definition. But $f_{a\,\mathrm{coord}}$ is equal to 96% in the case of a fully amorphous cell obtained by a melting-quench process, the discrepancy is

therefore limited. This definition will enable us to compare the atomistic results with the elastic results since in the latter the amorphous area is characterized by elastic and density properties different from the crystalline ones. It is reasonable to assume that these properties depend at the atomic scale on the nature and number of interatomic interactions, i.e. on the atomic coordination properties. Furthermore, as seen in the description of the elastic calculations the parameter considered in these calculations is the initial volumic amorphous fraction. This fraction is equal to the initial atomic fraction since the densities of the crystalline and amorphous materials are equal before volume relaxation. To enable the comparison with the elastic results the coordination amorphous fraction is then determined before relaxation. In these conditions:

$$f_{a\,\mathrm{coord}} = \phi^0(\mathrm{elastic}). \tag{6}$$

We then calculate the amorphous fraction as the ratio of the number of amorphous atoms over the total number of atoms in the simulation box. Both the coordination and lattice amorphous fractions are estimated, compared, and the swelling as a function of both amorphous fractions is determined.

3 Results on swelling as a function of the amorphous fraction

3.1 Swelling as a function of $f_{a_{\mathrm{lattice}}}$: comparison with experiments

No qualitative difference, and very slight quantitative differences are observed in the swelling induced by the introduction of a cubic or spherical amorphous zone. In the following we will discuss the results obtained in the case of the spherical *in situ* melted-quenched amorphous zone. Figure 4 shows the relative volume change $\Delta V/V^0$ as a function of the disorder amount determined after relaxation (a) in our Molecular Dynamics simulations in the case of spherical *in situ* melted-quenched amorphous zones, and (b) in the ion implantation experiments by Nipoti et al. [3].

On the experimental curve the disorder amount is expressed as the integral of displaced atoms. This parameter is determined from Rutherford Back Scattering spectra using various channeling approximations, and is assumed to be proportional to the fraction of amorphous material. We have compared these results with the volume variation as a function of $f_{a\,\mathrm{lattice}}$. The Molecular Dynamics results compare very well with the experimental curve. Two different regimes with similar relative slopes are observed in the two curves. This is consistent with the results of the preliminary study [15]. The linear scaling laws giving the swelling as a function of the lattice amorphous fraction for the two regimes are as follows:

$$\text{For } f_{a_{\mathrm{lattice}}} \leq 30.5\%, \Delta V/V^0 = 6.62.10^{-2} f_{a_{\mathrm{lattice}}} \tag{7}$$

$$\text{For } f_{a_{\mathrm{lattice}}} > 30.5\%, \Delta V/V^0 = 0.1105 f_{a_{\mathrm{lattice}}} - 1.351. \tag{8}$$

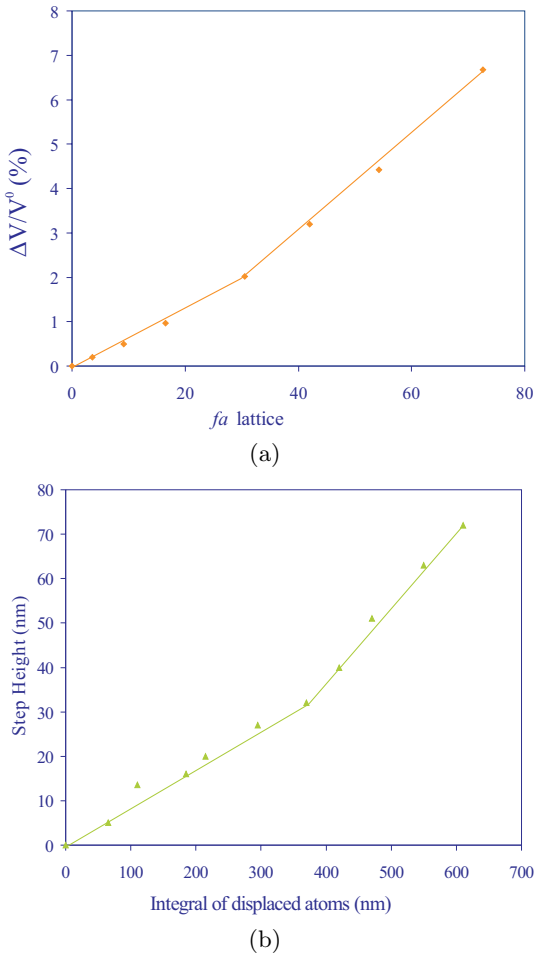

Fig. 4. Comparison of swelling as a function of $f_{a\,\mathrm{lattice}}$ yielded by (a) Classical Molecular Dynamics in the case of the spherical amorphous zone, and (b) in the ion implantation and RBS experiments by Nipoti [3].

As a conclusion, the model of the irradiation effect in two steps is reasonable, and the empirical Tersoff potential yields good results for the systems considered. Finally, the melting-quench amorphization enables us to reproduce the experimental results.

We have then analyzed our results as a function of the coordination amorphous fraction $f_{a\,\mathrm{coord}}$. Since this fraction relies on chemical and coordination criteria this will enable us to get further insight into the mechanisms involved in swelling and on the chemical evolution during this swelling.

3.2 Swelling as a function of $f_{a_{\mathrm{coord}}}$: comparison with the elastic model

The coordination amorphous fraction is the adequate definition to compare the atomistic and elastic approaches. Furthermore, the elastic calculations consider a spherical amorphous inclusion, and the elastic constants and densities have been computed using a melted-quenched

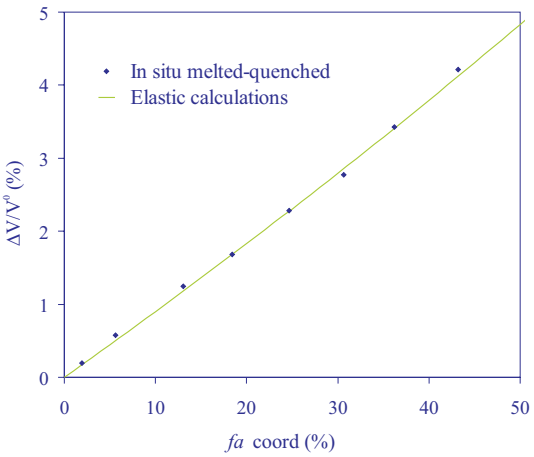

Fig. 5. Comparison of swelling as a function of $f_{a_{\text{coord}}}$ yielded by Classical Molecular Dynamics and elastic calculations.

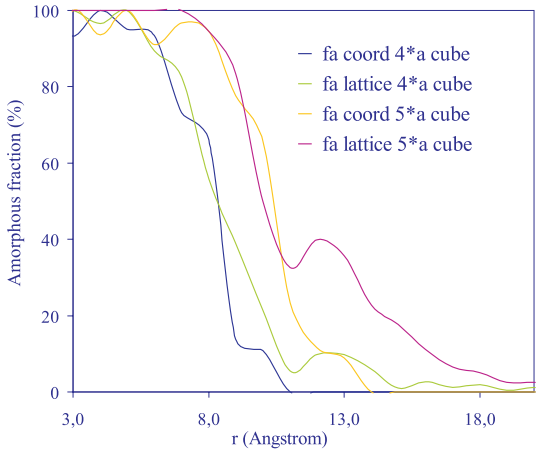

Fig. 6. Variations of the two amorphous fractions throughout the simulation box for two sizes of cubic amorphous zones.

amorphous material. We have therefore compared the elastic results to the Molecular Dynamics results obtained in the case of spherical in situ melted-quenched amorphous zones. Figure 5 shows the volume change as a function of the amorphous fraction yielded by the elastic calculations and the Molecular Dynamics simulations.

As can be seen on this figure the two methods are in excellent agreement. Furthermore, the coordination amorphous fraction remains approximately constant during volume relaxation. These two results suggest an elastic behavior of the material during relaxation. An elastic behavior had been excluded in the preliminary study [15] because it was unable to reproduce the two swelling regimes observed in the channeled RBS experiments. The use of two different definitions of the amorphous fraction introduced has therefore enabled us to reconcile the results of the available experiments with those of the elastic calculations. Given the very good agreement between the elastic and Molecular Dynamics results, the elastic law is chosen for the scaling law giving the swelling as a function of the coordination amorphous fraction. The resulting law obtained in replacing the values from Table 1 in equation (4) is as follows:

$$\frac{\Delta V}{V^0} = \frac{\alpha\, f_{a_{\text{coord}}}}{\beta + \gamma\, f_{a_{\text{coord}}}}, \tag{9}$$

with $\alpha = 9.3744 \times 10^4$, $\beta = 1.24074 \times 10^6$ and $\gamma = -3.4866 \times 10^5$.

3.3 Difference of behavior as a function of the two amorphous fractions

There is an apparent contradiction between the results as a function of the lattice and amorphous fractions. If we look more closely into the difference between the two definitions, it is first observed that $f_{a_{\text{lattice}}}$ is larger than $f_{a_{\text{coord}}}$ for all $f_{a_{\text{coord}}}$. The absolute difference between $f_{a_{\text{lattice}}}$ and $f_{a_{\text{coord}}}$ is between 10 and 20%, and is therefore larger than the small difference observed in the totally amorphized material. This means that a significant number of atoms shifted from their ideal lattice sites keep a crystalline coordination. Second, the relative difference $\Delta f_a/f_a$ defined as $(f_{a\text{lattice}} - f_{a\text{coord}})/f_{a\text{coord}}$ decreases when the amorphous fraction increases. Two regimes are observed in the $\Delta f_a/f_a$ variation as a function of $f_{a_{\text{coord}}}$: one with large slope for small amorphous fractions, and a second one for large amorphous fractions with a smaller slope. These two regimes explain why the swelling exhibits two regimes as a function of the lattice amorphous fraction, but only one as a function of the coordination amorphous fraction.

Figure 6 represents the variations of the two amorphous fractions throughout the simulation box for two sizes of cubic in situ amorphous zones.

It is seen that the differences between the two definitions are concentrated in the interface between the amorphous and the crystalline areas. This is confirmed by the visual analysis of the atomic configurations done with the AtomEye software [22]. This explains why the relative difference decreases with increasing amorphous fraction, since the relative proportion of atoms at the interface decreases when the size of the amorphous area increases. This also shows that the differences observed in the experimental and elastic results are derived from the difference in the description of the interface area. The lattice amorphous fraction describes the interface as larger and more amorphous, while the coordination amorphization fraction shows it to be more localized and crystalline. In the case of the introduction of a cubic amorphous zone, natural crystallographic directions are respected, and less four-time coordinated atoms are displaced from their ideal lattice site than in the case of a spherical amorphous zone. The difference between the two definitions is then smaller.

4 Conclusion

The introduction of an amorphous area in crystalline β-SiC through irradiation and the induced swelling have been investigated using classical Molecular Dynamics. The

swelling has been studied as a function of the amorphous fraction introduced.

Comparison with the experiments proves that the modeling chosen for the local amorphization is reasonable, and that the empirical Tersoff potential yields good results for the systems considered. Comparison with an elastic model shows that the amorphization-induced swelling exhibits an elastic behavior. This result should be confirmed by a thorough analysis of the disorder created and its evolution during relaxation.

The results yielded by the use of two different definitions for the amorphous fraction introduced underlines the crucial importance of the definition of the amorphous state at the atomic scale. This definition must be precise and adapted to the phenomena investigated. Furthermore, scalings for the swelling as a function of the two amorphous fractions considered, which can be used by larger scale models, have been determined. Finally, our study shows that Classical Molecular Dynamics calculations enable one to connect the results of the available experiments with the elastic calculations and to get further insight into the swelling mechanisms.

Appendix A: Elastic modeling

The equilibrium equation of a homogeneous isotropic hollow sphere with an internal pressure p_a can be found in basic books of Mechanics. Landau and Lifshitz [23] for instance give the displacement field u within the hollow sphere as a function of the radius r in the sphere. It depends on the internal and external radii, the Young modulus E_c, and the Poisson coefficient ν_c of the sphere. Using the same notations as in Section 2.5 where the superscripts 0 and f denote the initial and final states of the system the expression of u reads:

$$u = r^f - r^0 = a\, r^0 + \frac{b}{r^{0\,2}} \tag{10}$$

$$\text{with} \quad a = \frac{p_a\, {R_a^0}^3}{{R_c^0}^3 - {R_a^0}^3}\, \frac{1-2\,\nu_c}{E_c} \tag{11}$$

$$\text{and} \quad b = \frac{p_a\, {R_a^0}^3\, {R_c^0}^3}{{R_c^0}^3 - {R_a^0}^3}\, \frac{1+\nu_c}{E_c}. \tag{12}$$

Applying this formula to the internal and external radii R_a and R_c, with the help of the definition of ϕ^0 given by equation (3) and of the correspondences between elastic parameters for an isotropic material:

$$G_c = \frac{E_c}{2\,(1+\nu_c)} \tag{13}$$

$$K_c = \frac{E_c}{3\,(1-2\,\nu_c)}, \tag{14}$$

we obtain the expression of the radius changes as follows:

$$R_c^f = R_c^0 \left[1 + \frac{p^a}{1-\phi^0}\left(\frac{\phi^0}{3K_c} + \frac{\phi^0}{4G_c}\right)\right] \tag{15}$$

$$R_a^f = R_a^0 \left[1 + \frac{p^a}{1-\phi^0}\left(\frac{\phi^0}{3K_c} + \frac{1}{4G_c}\right)\right]. \tag{16}$$

Equation (15) enables us to obtain the total swelling:

$$\begin{aligned}\frac{\Delta V}{V^0} &= \frac{V^f - V^0}{V^0} = \left(\frac{R_c^f}{R_c^0}\right)^3 - 1 \approx 3\,\frac{R_c^f - R_c^0}{R_c^0} \\ &= \frac{\phi^0}{(1-\phi^0)}\left(\frac{3}{4\,G_c} + \frac{1}{K_c}\right) p^a,\end{aligned} \tag{17}$$

and equation (16) the swelling of the amorphous sphere:

$$\begin{aligned}\frac{V_a^f}{V_a^0} &= \left(\frac{R_a^f}{R_a^0}\right)^3 \approx 1 + 3\left(\frac{R_a^f - R_a^0}{R_a^0}\right) \\ &= 1 + \frac{1}{(1-\phi^0)}\left(\frac{3}{4\,G_c} + \frac{\phi^0}{K_c}\right) p^a.\end{aligned} \tag{18}$$

Furthermore, mass is conserved in the amorphous sphere during volume relaxation, so that:

$$\rho_a^f V_a^f = \rho_c^r V_a^0. \tag{19}$$

Combined with equation (18), it yields:

$$\frac{\rho_c^r}{\rho_a^f} = 1 + \frac{1}{(1-\phi^0)}\left(\frac{3}{4\,G_c} + \frac{\phi^0}{K_c}\right) p^a. \tag{20}$$

Let now V_a^r be the volume of the amorphous sphere at rest, that is the volume the amorphous sphere would have without pressure ($p_a = 0$). It is related to the corresponding amorphous density ρ_a^r by the expression:

$$\rho_a^f V_a^f = \rho_a^r V_a^r. \tag{21}$$

This equation allows us to write the amorphous constitutive equation in terms of densities:

$$p^a = -K_a\left(\frac{V_a^f - V_a^r}{V_a^r}\right) = -K_a\left(\frac{\rho_a^r}{\rho_a^f} - 1\right), \tag{22}$$

where K_a is the amorphous bulk modulus.

The combination of equations (20), (22), and (17) finally gives the pressure p_a and the total swelling as functions of the initial volumic amorphous fraction ϕ^0:

$$p_a = \frac{(1-\phi^0)\,(\rho_c^r - \rho_a^r)\,4\,K_a\,G_c\,K_c}{\rho_c^r\,(1-\phi^0)\,4\,G_c\,K_c + K_a\,\rho_a^r\,(3\,K_c + 4\,G_c\,\phi^0)} \tag{23}$$

$$\frac{\Delta V}{V^0} = \frac{\phi^0\,(\rho_c^r - \rho_a^r)\,K_a\,(3\,K_c + 4\,G_c)}{\rho_c^r\,(1-\phi^0)\,4\,G_c\,K_c + K_a\,\rho_a^r\,(3\,K_c + 4\,G_c\,\phi^0)}. \tag{24}$$

References

1. W.J. Weber, R.C. Ewing, C.R.A. Catlow, T. Diaz de la Rubia, L.W. Hobbs, C. Kinoshita, H. Matzke, A.T. Motta, M. Nastasi, E.K.H. Salje, E.R. Vance, S.J. Zinkle, J. Mater. Res. **13**, 1434 (1998)
2. W. Bolse, J. Conrad, T. Rödle, T. Weber. Surf. Coat. Technol. **927**, 74 (1995)
3. R. Nipoti, E. Albertazzi, M. Biancon, R. Lotti, G. Lulli, M. Cervera, A. Carnera, Appl. Phys. Lett. **70**, 3425 (1997)

4. R. Devanathan, T. Diaz de la Rubia, W.J. Weber, J. Nucl. Mater. **253**, 47 (1998)
5. R. Devanathan, W.J. Weber, F. Gao, J. Appl. Phys. **90**, 2303 (2001)
6. F. Gao, M. Posselt, V. Belko, Y. Zhang, W.J. Weber, Nucl. Instr. and Meth. B **218**, 74 (2004)
7. F. Gao, W.J. Weber, M. Posselt, V. Belko, Phys. Rev. B **69**, 245205 (2004)
8. C. Wang, J. Bernholc, R.F. Davis, Phys. Rev. B **38**, 12752 (1988)
9. W. Windl, T.J. Lenovsky, J.D. Kress, A.F. Voter, Nucl. Instr. and Meth. B **141**, 61 (1998)
10. F. Gao, E.J. Bylaska, W.J. Weber, L.R. Corrales, Phys. Rev. B **64**, 245208 (2001)
11. M. Bockstedte, A. Mattausch, O. Pankratov, Phys. Rev. B **68**, 205201 (2003)
12. G. Lucas, L. Pizzagalli, Nucl. Instr. and Meth. B **229**, 359 (2005)
13. Xianglong Yuan, Linn W. Hobbs, Nucl. Instr. and Meth. B **191**, 74 (2002)
14. F. Gao, W.J. Weber, J. Mater. Res. **18**, 1877 (2003)
15. A. Romano, M. Bertolus, M. Defranceschi, S. Yip, Nucl. Instr. and Meth. B **202**, 100 (2003)
16. J. Tersoff, Phys. Rev. B **39**, 5566 (1989)
17. J. Li, L.J. Porter, S. Yip, J. Nucl. Mater. **246**, 53 (1997)
18. R. Devanathan, W.J. Weber, T. Diaz de la Rubia, Nucl. Instr. and Meth. B **141**, 118 (1998)
19. J.M. Perlado, L. Malerba, A. Sanchez-Rubio, T. Diaz de la Rubia, J. Nucl. Mater. **276**, 235 (2000)
20. J. Rifkin, `http://xmd.sourceforge.net`, 2004
21. J. Tersoff, Phys. Rev. B **49**, 16349 (1994)
22. J. Li, Modelling Simul. Mater. Sci. Eng. **11**, 173 (2003)
23. L. Landau, E. Lifshitz, Theory of elasticity, *Course of Theoretical Physics*, 3rd edn. (Butterworth-Heinemann, 1986), Vol. 7